energies

MDPI

Article

Quantitative Characterization of Surfactant Displacement Efficiency by NMR—Take the Tight Oil of Chang 8 Member of Yanchang Formation in Fuxian Area, Ordos Basin, as an Example

Hu Yin [1,2], Gaorun Zhong [3,*], Jiangbin Liu [3] and Yanjun Wu [3]

[1] State Key Laboratory for Continental Dynamics, Department of Geology, Northwest University, Xi'an 710069, China; huy19878825@126.com
[2] Fuxian Oil Production Plant, Yanchang Oilfield Co., Ltd., Fu'xian 727500, China
[3] School of Petroleum Engineering and Environmental Engineering, Yan'an University, Yan'an 716000, China; liujiangbin163@163.com (J.L.); wuyanjun_217@163.com (Y.W.)
* Correspondence: zhongaorun@126.com

Abstract: Surfactant flooding is a pivotal technique for enhancing oil recovery efficiency. The Chang 8 member of the Yanchang Formation in the Ordos Basin exemplifies a quintessential tight oil reservoir. Specifically, 47.9% of wells yield less than 0.1 t/d, 27.0% produce between 0.1 and 0.2 t/d, and 18.8% generate outputs ranging from 0.2 to 0.3 t/d, while only a mere 6.3% exceed production rates of over 0.3 t/d, indicating minimal efficacy of water flooding development in this context. In this study, we conducted an extensive investigation into the geological characteristics of the Yanchang 8 reservoir within the Ordos Basin, leading to the identification and evaluation of three surfactants based on their interfacial tension properties. The optimal injection concentration was determined through on-line displacement nuclear magnetic resonance imaging analysis that refined surface activity conducive to developing the Chang 8 member, ultimately resulting in increased spread volume and enhanced crude oil production from individual wells. The results indicate the following: (1) The interfacial tension of NP-10, FSD-952, and GPHQ-1 at concentrations of 0.05%, 0.1%, 0.2%, 0.3%, 0.4%, and 0.5% exhibited a pattern of initial decrease followed by an increase. The mass concentration corresponding to the minimum interfacial tension for NP-10 is identified as 0.1%, which is also the case for GPHQ-1; however, for FSD-952, this occurs at a concentration of 0.4%. Among the surface-active agents NP-10, GPHQ-1, and FSD-952, GPHQ-1 demonstrated the lowest interfacial tension value at an impressive measurement of 0.0762 mN/m. (2) When the displacement of the 0.1% GPHQ-1 surfactant reaches 10 PV, the displacement efficiency improves from 69.69% to 76.36%, representing an increase of 6.67%. The minimum pore size observed during GPHQ-1 surfactant displacement is 0.01 μm. In contrast, when the displacement of the NP-10 surfactant at a concentration of 0.1% reaches 10 PV, the efficiency rises from 68.32% to 72.02%, indicating an enhancement of 3.7%. The corresponding minimum pore size for NP-10 surfactant displacement is recorded at 0.02 μm. Furthermore, when the displacement of the FSD-952 surfactant at a concentration of 0.4% achieves 10 PV, its efficiency increases from 69.93% to 74.77%, reflecting an improvement of 4.81%. The minimum pore size associated with the activated portion of FSD-952 is noted as being approximately 0.03 μm.

Keywords: surfactant; low permeability reservoir; oil recovery efficiency; nuclear magnetic resonance; Ordos Basin

check for updates

Citation: Yin, H.; Zhong, G.; Liu, J.; Wu, Y. Quantitative Characterization of Surfactant Displacement Efficiency by NMR—Take the Tight Oil of Chang 8 Member of Yanchang Formation in Fuxian Area, Ordos Basin, as an Example. *Energies* **2024**, *17*, 5450. https://doi.org/10.3390/en17215450

Academic Editor: Vladimir Alvarado

Received: 12 October 2024
Revised: 28 October 2024
Accepted: 29 October 2024
Published: 31 October 2024

Copyright: © 2024 by the authors. Licensee MDPI, Basel, Switzerland. This article is an open access article distributed under the terms and conditions of the Creative Commons Attribution (CC BY) license (https://creativecommons.org/licenses/by/4.0/).

1. Introduction

In the context of oil displacement, a variety of physical and chemical transformations occur between the aqueous solution, crude oil, and reservoir. These transformations not only enhance fluid properties but also optimize reservoir characteristics, thereby facilitating improved oil recovery [1]. The principal surfactants utilized in oil displacement comprise naturally modified surfactants and synthetic derivatives. The primary classifications

include non-ionic, anionic, cationic, amphoteric, Gemini, biological, fluorocarbon, and polymer surfactants. Anionic surfactants are extensively employed; zwitterionic and non-ionic formulations are also widely recognized. Currently under exploration are Gemini surfactants and biosurfactants. Cationic surfactants exhibit limited applicability [2–12].

Comprehensive research and field trials on enhanced oil recovery via nano flooding have been rigorously undertaken in the Changqing, Yanchang, and Bohai oilfields. In October 2018, Changqing oilfield undertook a pilot test of the "10 injection and 36 production" methodology in the Jiyuan ultra-low permeability reservoir, which predominantly exhibited characteristics of enhanced fluid influx, increased oil recovery, and subsequent decline. In the peripheral ultra-low permeability tight reservoirs of the Daqing oilfield, nuclear magnetic resonance (NMR) techniques have been utilized to perform core experimental investigations within a nano-flooding chamber, leading to a marked improvement in recovery rates. Yanchang Oilfield Company undertook a field trial of the "2 injection 11 production" super nano strong displacement agent within the Yongjin 103 and Yongjin 198 well groups at Zhidan oilfield, which yielded a notable 19.8% enhancement in output from effective wells. A field trial of the "1 injection and 4 production" nanometer microball displacement agent was conducted in the QSS-46 well group of Wuqi oilfield. Subsequent to its application, the injection pressure at the well experienced a reduction of 40%, while daily oil production increased from 5.9 tons to 6.9 tons, reflecting an enhancement of 17%. Furthermore, the water cut decreased from 70% to 56.6%. CNOOC has undertaken comprehensive research and the application of nano-flooding technology in both the Bohai Q oilfield and Penglai 19-3 oilfield. Importantly, a systematic evaluation of nano-dispersible flooding was conducted on a cohort of oil wells within the Bohai normal heavy oil Q oilfield, leading to a water cut reduction ranging from 3% to 10%.

Wang Chengjun (2018) utilized reservoir screening and evaluation methodologies to investigate the compatibility of surfactant flooding in Yanchang Formation reservoirs located within the Ordos Basin [13]. The results revealed that 57 out of 210 blocks exhibited a low comprehensive evaluation value, specifically below 0.5, whereas 153 blocks were identified as more suitable for surfactant flooding [14]. According to the available data, surfactant flooding can markedly enhance the recovery rate, exhibiting substantial potential for optimizing oil recovery in the Yanchang Formation [15–20]. Compared to water flooding, surfactant flooding exhibits a markedly enhanced oil recovery (EOR) potential in high water cut reservoirs of the Chang 8 member within the Yanchang Formation, Ordos Basin. This phenomenon can be primarily attributed to the advanced stage of water drive development in these reservoirs, which has led to diminishing efficacy in further improving oil recovery through continuous water drive methods. In contrast, surfactant flooding effectively mobilizes residual hydrocarbons and significantly enhances overall oil recovery.

Du et al. (2024) utilized nuclear magnetic resonance techniques to perform dynamic seepage experiments on tight oil and shale oil in conjunction with matrix fractures, thereby elucidating the distribution characteristics of residual oil throughout the dynamic imbibition process [21]. Bai et al. (2016) and Zhong et al. (2024) conducted a thorough examination of the quantitative characterization techniques for NMR T2 spectroscopy in sandstone rocks, elucidating their significance in petroleum exploration and development [22,23]. Li et al. (2024) conducted a comprehensive study on the sand transport behavior and molecular dynamics of water-based fracturing fluids within fractures of shale reservoirs [24]. Li et al. (2024) conducted a numerical investigation into blowout control utilizing the displacement kill method during well testing of deepwater gas reservoirs [25].

The study area is located within the Fuxian region of the Ordos Basin, covering an expanse of 18 km^2. It comprises 17 water injection wells, 63 production wells, and 14 shut-in wells. The primary oil production rate is recorded at 80.83 tons per day, while the primary liquid production rate is measured at 193.22 cubic meters per day. Prior to the initiation of water injection in 2019, oil production was documented at 11.3 tons per day, while liquid production was measured at 14 cubic meters per day. Following the commencement of water injection in 2019, the maximum monthly volume injected

was constrained to a mere 217 cubic meters per day, with an injection pump pressure recorded at 17 MPa and a wellhead pressure noted at 13.5 MPa. Following five years of water injection, the current daily oil production is recorded at 6 tons, accompanied by a total fluid output of 8.0 cubic meters per day. Notably, 47.9% of wells produce less than 0.1 tons per day, while 27.0% yield between 0.1 and 0.2 tons per day; an additional 18.8% generate between 0.2 and 0.3 tons per day, with only a modest fraction of 6.3% exceeding a production rate of 0.3 tons per day. The efficacy of the water flooding development appears to be constrained, suggesting a limited impact from the water flooding process. In this study, a thorough investigation of the geological characteristics of the Chang 8 reservoir in the Ordos Basin was conducted, leading to the identification of three surfactants for further evaluation. The interfacial tension was systematically measured to ascertain the optimal injection concentration, followed by an advanced on-line displacement nuclear magnetic resonance imaging analysis. This methodology effectively optimized surface activity conducive to the development of the Chang 8 member, thereby enhancing both the spread volume and the crude oil production from individual wells.

2. Experiments

The sedimentary period of the Chang 8 member in the Fuxian area of the Ordos Basin is defined by a deltaic sedimentary environment, predominantly comprising lithic arkose and arkose as its primary rock types. The clay mineral assemblage exhibits a chlorite content exceeding 40%, followed by illite/montmorillonite interlayers at approximately 25%, illite around 20%, and kaolinite constituting less than 5%. The average core porosity ranges from 7.0% to 10.0%, while the average permeability is (0.01 to 0.25) $\times$ 10^{-3} μm^2, categorizing it as a low-porosity and ultra-low-permeability reservoir. Microscopic slice analysis reveals that the pore types in the Chang 8 member reservoir are predominantly intergranular pores, accompanied by a limited occurrence of fracture pores and intergranular micropores. Additionally, MRI and CT scan results demonstrate that the core possesses a relatively high density, characterized by 14.5% microthroat type, 3.5% microfracture development type, and 82% micropores. Fluorescence analysis reveals that in the tight sandstone of Chang 8 within the Yanchang Exploration area, oil is predominantly concentrated in intergranular pores, cutting-dissolving pores, and intergranular dissolving pores, primarily manifesting as an emulsion. The average surface crude oil density of Chang 8 is recorded at 0.828 g/cm^3, which falls below the critical threshold of 0.84 g/cm^3, thereby classifying it as light crude oil. The dynamic viscosity at 50 °C is approximately 3.6 mPa·s. The dominant formation water type is $CaCl_2$, reflecting optimal sealing conditions, with an average total salinity of 15,234.76 mg/L.

The interfacial tension of the surfactant samples was evaluated, specifically for NP-10, FSD-952, and GPHQ-1.

NP-10: Molecular formula: $C_9H_{19}C_6H_4(OCH_2CH_2)10OH$; Common name: Nonylphenol Ethoxylate (10 moles). The NP-10 experimental analysis samples were supplied by Jinan Baoliyuan Chemical Co., Ltd, Jinan, China. The effective content is 99%, presenting as a colorless and transparent liquid, with a turbidity point of 60 to 67 °C, and a pH value ranging from 6.0 to 7.0.

FSD-952: A perfluoroalkyl alcohol devoid of PFOS and PFOA, characterized by both non-ionic and anionic properties. The FSD-952 sample was supplied by Xinxiang Shengqing New Material Co., Ltd, Xinxiang, China. The concentration of the active ingredient is 45%, characterized by a uniform liquid appearance, with thermal stability up to 150 °C and a pH range of 6.0 to 8.0.

GPHQ-1: A nano-emulsion displacement agent exhibiting an average particle size of 5 nm. GPHQ-1 is provided by Sichuan Jiebeitong Energy Technology Co., Ltd, Suining, China. The concentration of the active ingredient is 75%, characterized by a light yellow, homogeneous liquid appearance. It exhibits thermal stability within the range of 80 to 150 °C, and maintains a pH value between 6.0 and 9.0.

The mass concentrations of surfactants were 0.05%, 0.1%, 0.2%, 0.3%, 0.4%, and 0.5%, respectively, with the experimental temperature maintained at 40 °C utilizing a rotary drop interfacial tensiometer.

The experimental analysis detailed in this paper was carried out at Suzhou Numai Technology Co., Ltd., Suzhou, China.

The principal analytical procedures and the selection of parameters for the experiment are outlined as follows:

Step 1: Initially, the oil and salt contained within the core sample are meticulously washed, followed by the execution of an NMR test subsequent to treatment. The porosity and permeability metrics are subsequently derived from the NMR analysis.

In the assessment of essential physical properties, eight core samples were meticulously selected, and their porosity and permeability were quantified utilizing nuclear magnetic resonance (NMR) techniques. The core samples are depicted in Figure 1.



Figure 1. Core sample (the core diameter was 2.5 cm).

Step 2: The sample underwent drying for 12 h at a temperature of 105 °C, following which the dry weight was measured and the original NMR T2 spectrum was acquired.

Step 3: In accordance with the NMR results, four core samples were identified for on-line displacement NMR imaging analysis.

In the analysis of on-line displacement imaging, a pre-treatment process was conducted. The instrument used for pre-treatment pressure was the HX-II vacuum pressure saturation apparatus. The instruments employed in the displacement experiment comprise the MacroMR12-150H-I, a large-scale nuclear magnetic resonance imaging analyzer specifically engineered for high-temperature and high-pressure applications, produced by NYMD Analytical Instruments Co., Ltd, Danyang, China. This apparatus operates at a resonance frequency of 12.798 MHz and exhibits a magnetic field strength of 0.3 T. The displacement coil has a diameter of 100 mm, while the maximum permissible sample diameter is limited to 25 mm; it functions optimally at a magnet temperature of 32 °C (Figure 2).

For the T_2 spectrum test parameters, CPMG sequence specifications include TW = 3500 ms, RG1 = 20 dB, DRG1 = 3, PRG = 2, SW = 200 kHz, NECH = 12000, TE = 0.15 ms, P1 = 11 μs, P2 = 18.48 μs, and NS = 16. The imaging test parameters for sagittal and cross-sectional imaging MRI include FOV read = 150 mm, FOV phase = 150 mm, TR = 500 ms, TE = 5.885 ms, slices = 1, slice width = 25 mm, slice gap = 0.5 mm, averages = 16, K space size = 192 × 256.

Sample saturation was conducted as follows: A vacuum pressure saturation device was employed to subject the sample to a vacuum of −0.1 MPa for a duration of 2 h. Subsequently, the saturated sample was extracted under pressure using saturated simulated oil (15 Pa) for 12 h, and the surface of the sample was cleaned with a damp paper towel. The T_2 spectrum and NMR image of the saturated sample were acquired using nuclear magnetic resonance equipment.

Step 4: A comprehensive on-line displacement NMR imaging analysis was performed for both the reference and experimental groups.

In the reference group, during the water displacement process at a constant flow rate of 0.2 mL/min, manganese chloride solution was introduced into the core. The production rates of oil and water were continuously monitored throughout the experiment. Data collection persisted until no additional oil was produced and there was no appreciable

decrease in T2 spectrum signal intensity. The T2 spectrum and imaging analyses were performed under saturated oil and water drive conditions at 1 PV, 3 PV, 5 PV, 10 PV, and 15 PV, respectively.



Figure 2. Experimental apparatus. (**a**) Nuclear magnetic resonance analysis system; (**b**) High-temperature and high-pressure circulation system; (**c**) NMR on-line displacement imaging system; (**d**) Back-pressure system; (**e**) Gas injection system and liquid injection system.

In the experimental group, an initial water displacement experiment was performed, subsequently followed by a surfactant displacement experiment, thereby facilitating a continuous displacement process.

During the water displacement experiment phase, a manganese chloride solution was injected into the core at a constant flow rate of 0.2 mL/min, while oil and water production were monitored throughout the process. T2 spectrum and imaging analyses were conducted under saturated oil and water displacement conditions at 1 pore volume (PV), 3 PV, and 15 PV, respectively.

Following the completion of the water displacement experiment, the surfactant displacement experiment commenced immediately, with core injection conducted under a constant flow rate of 0.2 mL/min. Throughout the experiment, oil and water production were monitored. T2 spectrum and imaging analyses were performed at surfactant displacements of 1 PV, 3 PV, 5 PV, and 10 PV, respectively.

3. Results and Discussion

The results of the physical property analysis for eight core samples are presented in Table 1. The NMR T_2 spectral characteristics are illustrated in Figure 3. Nuclear magnetic resonance findings indicate that the nuclear magnetic porosity ranges from 9.56% to 11.88%, while the weighing porosity varies between 10.04% and 12.48%. Additionally, permeability is measured at (0.0117~0.03789) $\times 10^{-3}$ μm^2.

The findings from the interfacial tension measurements reveal the following: (1) The interfacial tension exhibits an initial decrease followed by an increase at surfactant concentrations of 0.05%, 0.1%, 0.2%, 0.3%, 0.4%, and 0.5%, indicating the presence of an optimal surfactant concentration; (2) The mass concentration corresponding to the minimum interfacial tension for NP-10 is identified as 0.1%, whereas GPHQ-1 and FSD-952 reach their respective minimum interfacial tensions at concentrations of 0.1% and 0.4%; (3) Among the surface-active agents NP-10, GPHQ-1, and FSD-952, GPHQ-1 demonstrates the lowest recorded interfacial tension, quantified at 0.0762 mN/m. Table 2 and Figure 4 present the statistical data regarding the interfacial tension test results.

Table 1. Statistical table of core NMR parameters.

Sample Number	Dismantle the Saturated Semaphore System (a.u.)	Nuclear Magnetic Conver-sion of Water (g)	Sample Volume (cm^3)	Drying Quality (g)	Saturation Mass (g)	Saturated Water Mass (g)	Weighing Water Volume (cm^3)	Nuclear Magnetic Porosity (%)	Permeability ($\times 10^{-3}$ μm^2)
FX40-3	27,538.4249	2.6940	23.82	55.187	58.004	2.817	2.817	11.31	0.0364
FX40-4	24,473.6074	2.3942	25.04	59.070	61.583	2.513	2.513	9.56	0.0134
FX40-5	26,216.2458	2.5647	21.59	49.764	52.459	2.695	2.695	11.88	0.0282
FX40-6	27,040.7879	2.6454	24.92	58.106	60.881	2.775	2.775	10.62	0.0293
FX40-7	29,535.1240	2.8894	24.93	57.572	60.625	3.053	3.053	11.59	0.0353
FX40-8	29,352.0413	2.8715	24.84	57.535	60.577	3.042	3.042	11.56	0.0264
FX40-9	28,379.1914	2.7763	23.71	55.055	58.004	2.949	2.949	11.71	0.0379
FX40-10	24,985.8269	2.4443	25.17	59.190	61.762	2.572	2.572	9.71	0.0117

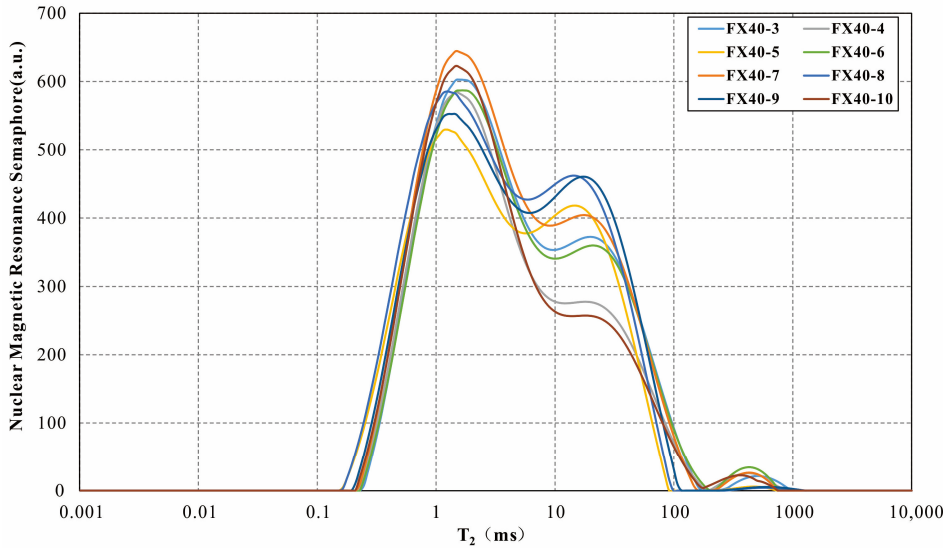

Figure 3. Core NMR T2 spectrum characteristics (saturated water).

Table 2. Statistical table for measurement of the interfacial tension of different surfactants.

Mass Concentration (%)	Interfacial Tension (mN/m)		
	NP-10	GPHQ-1	FSD-952
0.05	1.2789	5.8041	0.8116
0.1	0.5434	0.0762	0.3197
0.2	2.5823	0.2951	0.4919
0.3	4.5744	0.4919	0.3689
0.4	4.1317	1.4264	0.123
0.5	4.5484	2.1642	0.9592

A water drive experiment was conducted on the FX40-5 sample. At a water drive pore volume (PV) of 15 PV, the oil recovery efficiency remained constant, suggesting that the water drive efficiency had reached its maximum capacity. Throughout this process, T2 spectrum real outlet metering and on-line displacement NMR imaging analyses were undertaken. The findings of this study demonstrate that during the water flooding process, oil is primarily mobilized from medium-to-large pores. Upon achieving a cumulative water injection of 5 pore volumes (PV), there is a slight improvement in water flooding efficiency,

which is subsequently followed by the initiation of ineffective water flooding. At 15 PV, the maximum efficiency of water flooding reaches 68.45%, beyond which no further enhancement is observed. The statistical data regarding the efficiency of oil displacement through water drive are presented in Table 3. The diagram illustrating oil displacement efficiency can be found in Figure 5. The T2 spectrum is depicted in Figure 6. The characteristics of pore size related to oil displacement corresponding to various water drive PV numbers are illustrated in Figure 7. The on-line nuclear magnetic imaging characteristics associated with different water drive PV numbers are shown in Figure 8.

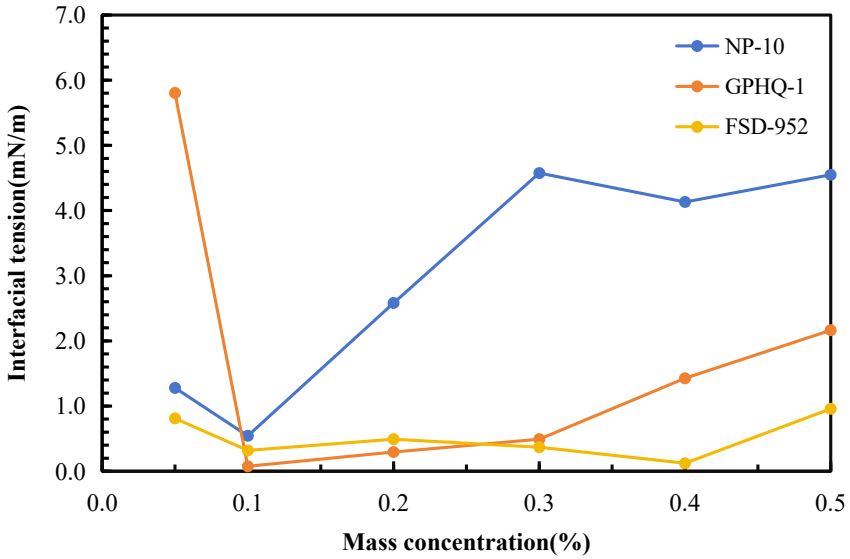

Figure 4. Results of interfacial tension measurements for various types of surfactants.

Table 3. Statistical analysis of oil displacement efficiency in water drive mechanisms.

Serial Number	Semaphore Signaling Mechanism	Displacement Efficacy (%)	Export Assessment
Saturated oil	12,232.50237		\
Water displacement: 1 PV	9959.651072	18.58	Oil: 0.5 mL; Water: 2.1 mL
Water displacement: 3 PV	6725.102383	45.02	Oil: 1.2 mL; Water: 6.7 mL
Water displacement: 5 PV	4867.58397	60.21	Oil: 1.6 mL; Water: 11.7 mL
Water displacement: 10 PV	3991.148893	67.37	Oil: 1.8 mL; Water: 25.1 mL
Water displacement: 15 PV	3859.676573	68.45	Oil: 1.9 mL; Water: 38.6 mL

For the FX40-7 samples, water displacement was initially performed, followed by the displacement of the GPHQ-1 surfactant at a mass concentration of 0.1%. Upon reaching a water displacement PV of 15 PV, the oil displacement efficiency remained constant, signifying that the water displacement efficiency had achieved its maximum threshold. At this juncture, the GPHQ-1 surfactant at a mass concentration of 0.1% was employed for the purpose of enhancing displacement. Under conditions characterized by saturated oil and varying PV values for displacement, T_2 spectrum real outlet metering alongside on-line nuclear magnetic resonance imaging investigations were performed. The results demonstrate that during the water displacement process, oil is primarily mobilized from medium-to-large pores. Upon achieving a water displacement of 5 pore volumes (PV), a marginal enhancement in the displacement efficiency is observed, coinciding with the initiation of ineffective water injection. At 15 PV, the maximum oil recovery efficiency reaches 69.69%. Following this, an experimental investigation employing the GPHQ-1 surfactant at a mass concentration of 0.1% was performed. Nuclear magnetic resonance T2 spectra and on-line nuclear magnetic imaging indicated that oil within smaller pores

began to be mobilized. When the GPHQ-1 surfactant displacement reached 10 PV, the oil recovery efficiency increased from 69.69% to 76.36%, reflecting an improvement of 6.67%. The minimum pore diameter of the crude oil utilized in the surfactant displacement process with GPHQ-1 is 0.01 μm. The statistical data regarding oil displacement efficiency are presented in Table 4. The diagram illustrating oil displacement efficiency can be found in Figure 9. The T2 spectrum is depicted in Figure 10. The pore diameter characteristics associated with varying displacement PV numbers are illustrated in Figure 11. Additionally, the on-line NMR imaging features corresponding to different displacement PV numbers are shown in Figure 12.

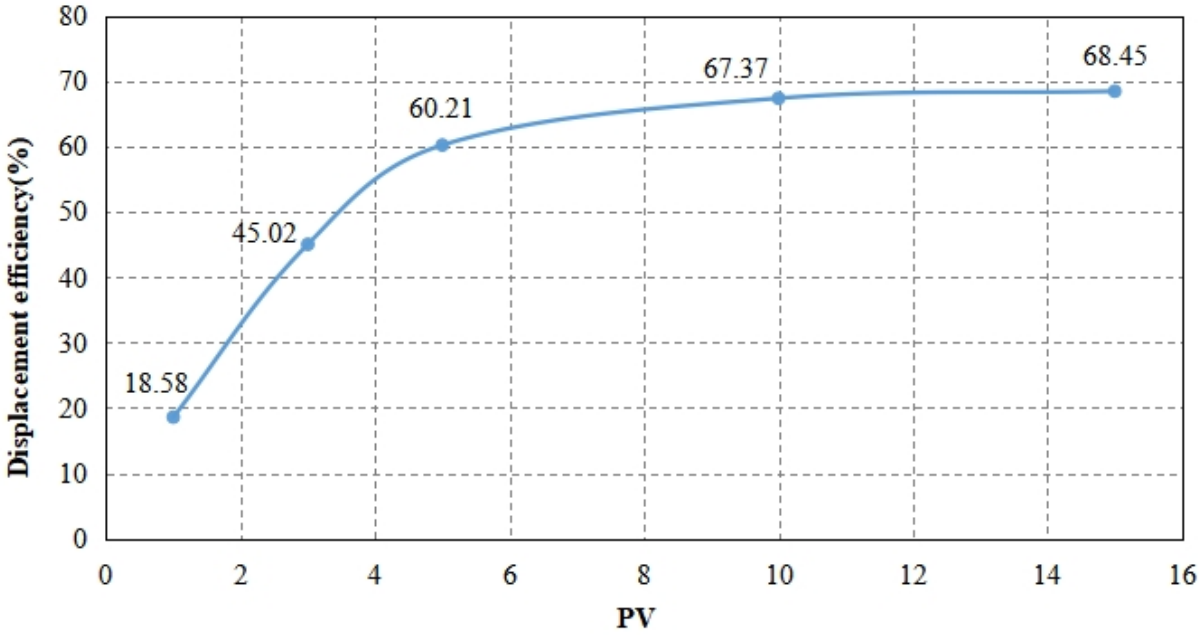

Figure 5. Diagram of water displacement efficiency.

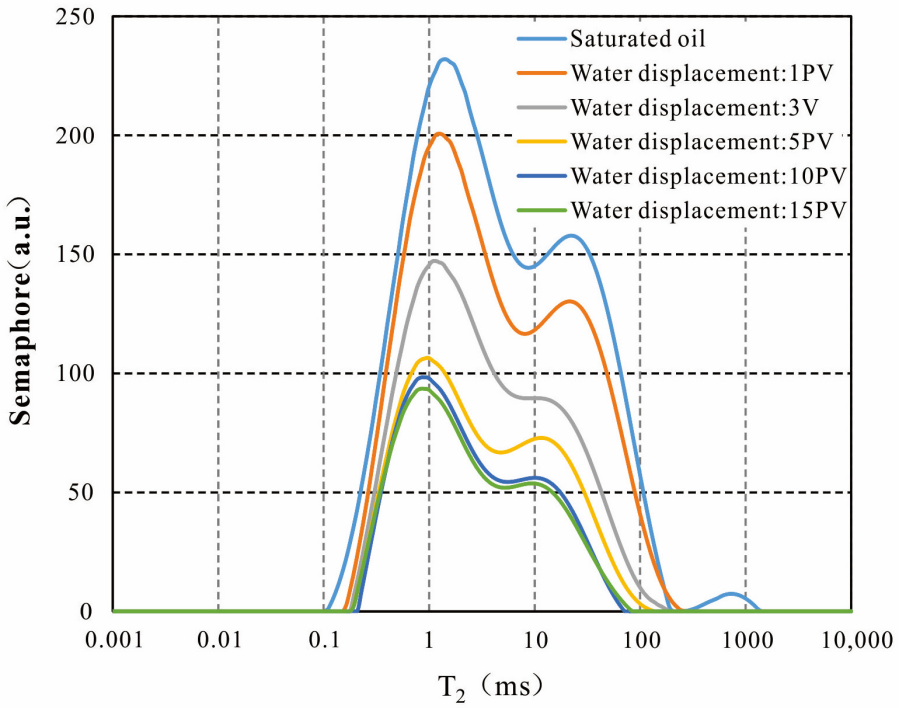

Figure 6. NMR T_2 spectral characteristics corresponding to the PV number of water displacement.

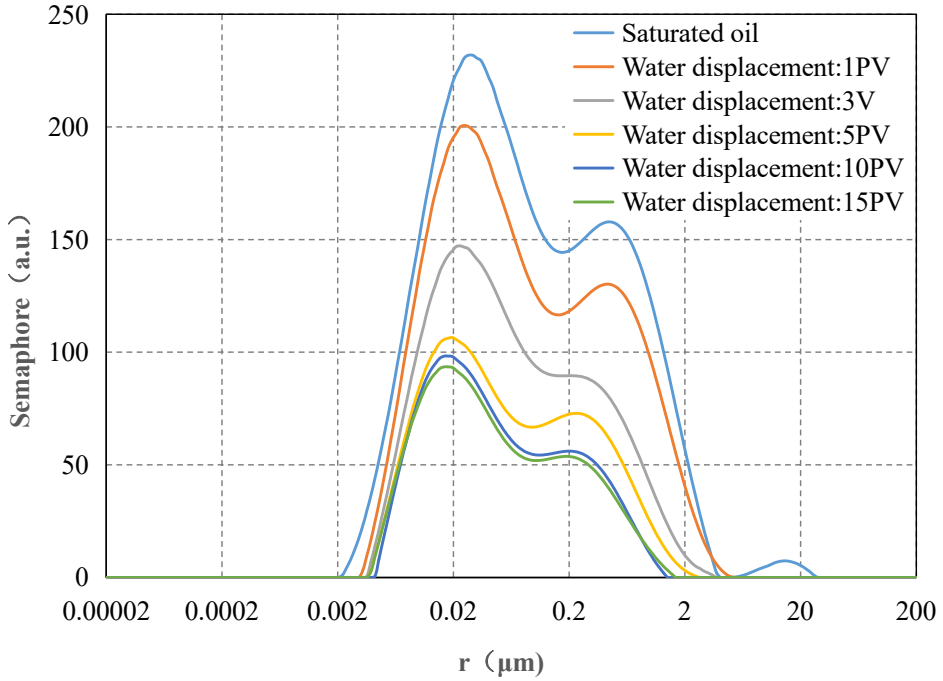

Figure 7. Characteristics of pore diameter related to water displacement as a function of PV number.

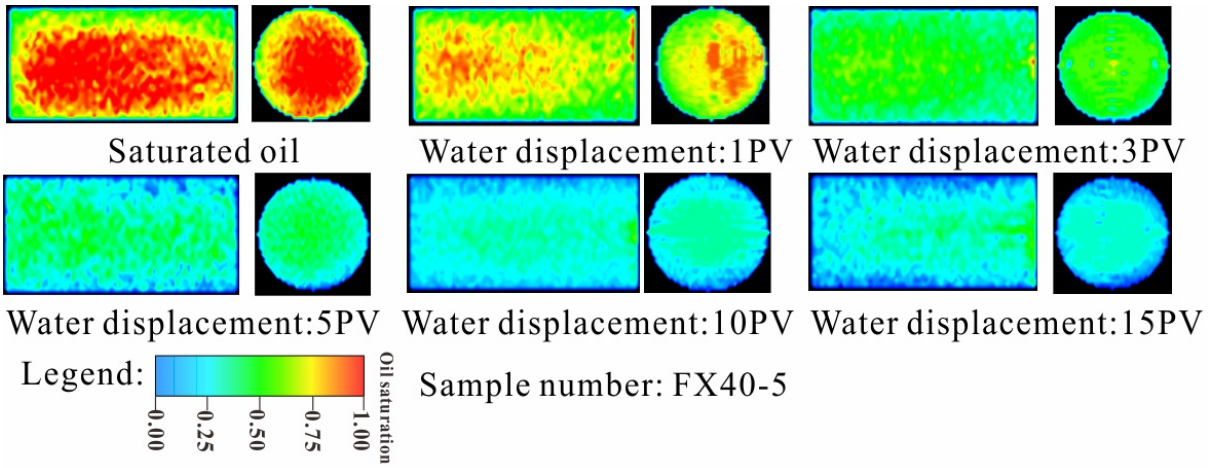

Figure 8. On-line displacement NMR imaging characteristics corresponding to different water displacement PV numbers.

Table 4. Statistical analysis of oil displacement efficiency.

Serial Number	Semaphore Signaling Mechanism	Displacement Efficacy (%)	Export Assessment
Saturated oil	13,140.52747	\	\
Water displacement: 1 PV	10,528.229	19.88	Oil: 0.6 mL; Water: 2.4 mL
Water displacement: 3 PV	6854.644385	47.84	Oil: 1.4 mL; Water: 7.6 mL
Water displacement: 15 PV	3982.990105	69.69	Oil: 2.0 mL; Water: 43.3 mL
GPHQ-1 displacement: 1 PV	3569.593656	72.84	Oil: 2.1 mL; Water: 45.8 mL
GPHQ-1 displacement: 3 PV	3336.725734	74.61	Oil: 2.2 mL; Water: 51.9 mL
GPHQ-1 displacement: 5 PV	3123.122055	76.23	Oil: 2.3 mL; Water: 57.9 mL
GPHQ-1 displacement: 10 PV	3105.888178	76.36	Oil: 2.3 mL; Water: 73.0 mL

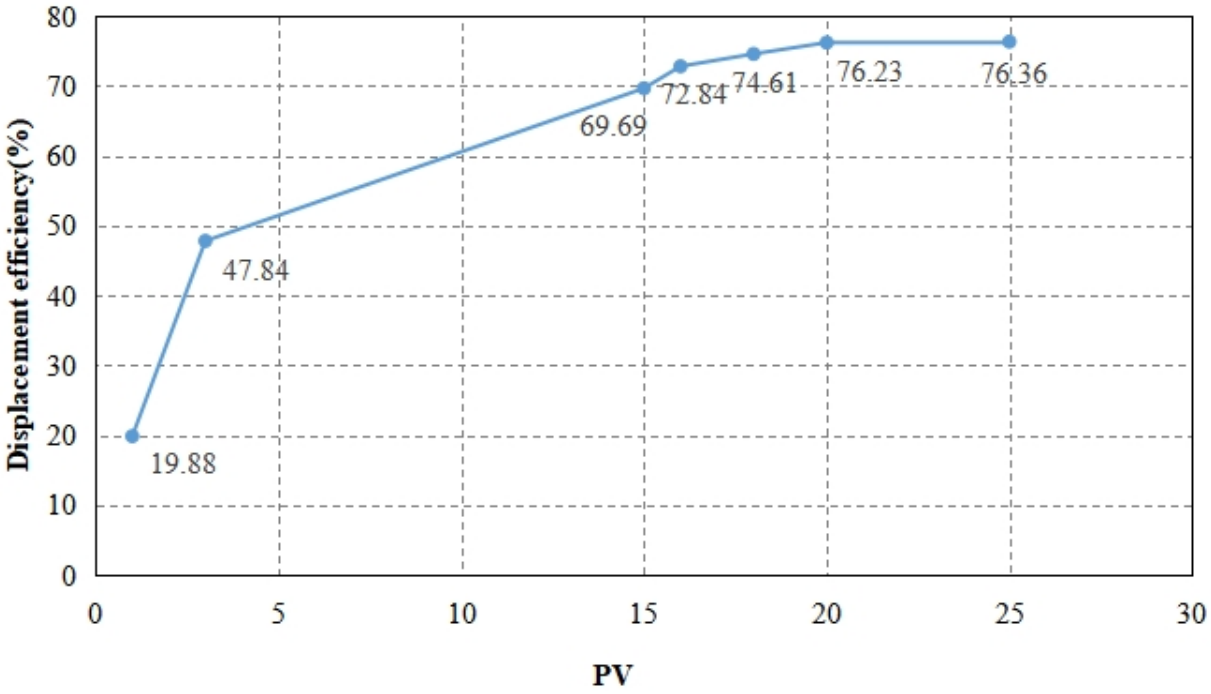

Figure 9. Displacement efficiency diagram for the "water displacement + GPHQ-1 surfactant displacement".

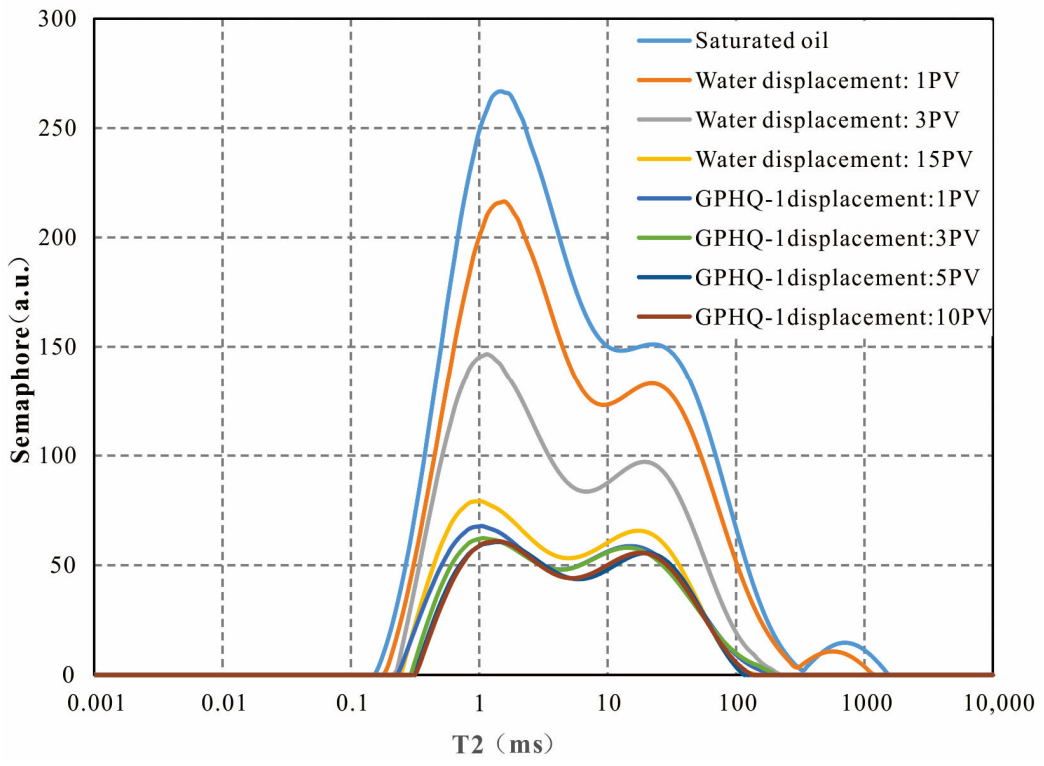

Figure 10. NMR T2 spectral characteristics corresponding to different PV numbers of "water displacement + GPHQ-1 surfactant displacement".

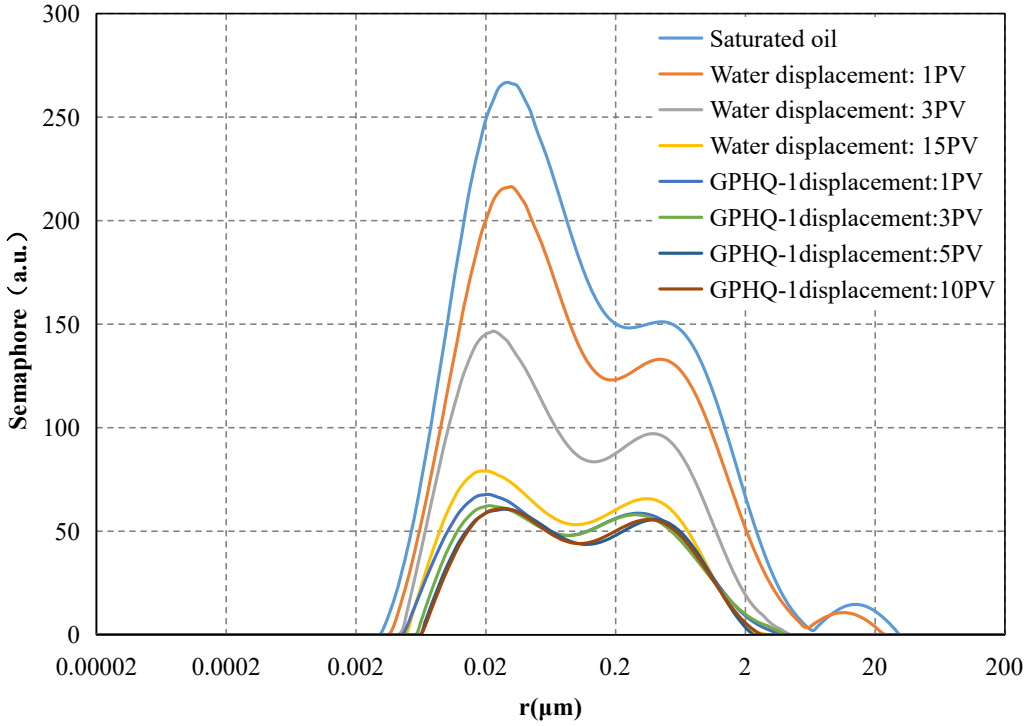

Figure 11. Oil displacement pore size characteristics corresponding to different PV numbers of "water displacement + GPHQ-1 surfactant displacement".

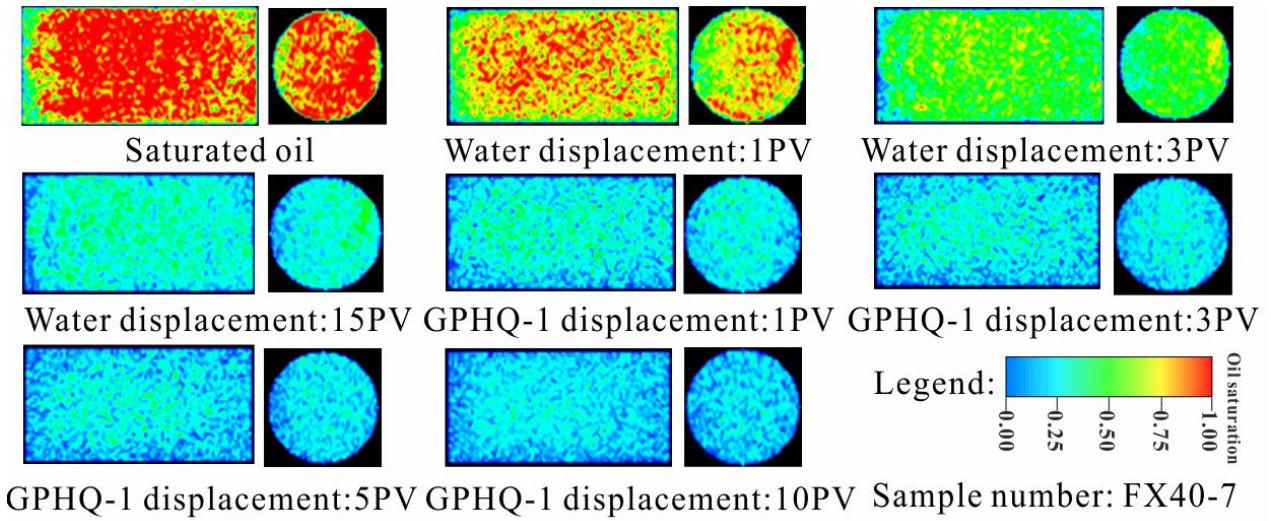

Figure 12. On-line NMR imaging characteristics corresponding to different PV numbers of "water displacement + GPHQ-1 surfactant displacement.

In the case of the FX40-8 samples, water displacement was initially performed, followed by NP-10 surfactant displacement at a concentration of 0.1%. Upon reaching a cumulative water drive PV value of 15 PV, no further changes in oil displacement efficiency were observed, indicating that the maximum water drive efficiency had been attained. At this stage, the displacement of NP-10 surfactant was initiated, and T2 spectrum real outlet metering, along with on-line displacement NMR imaging, were performed under conditions of saturated oil and varying displacement PV values. The results indicate that during the process of water displacement, oil predominantly resides in medium-to-large pores. When the displacement volume reaches 5 pore volumes (PV), there is a minimal improvement in the displacement efficiency. However, upon reaching a displacement volume

of 15 PV, the maximum displacement efficiency is achieved at 68.32%. Subsequently, the displacement of NP-10 surfactant at a mass concentration of 0.1% was conducted, resulting in the expulsion of oil from pores with diameters less than 0.02 μm, as evidenced by NMR T2 spectroscopy and on-line NMR imaging techniques. Upon achieving a displacement volume of 10 PV with the 0.1% NP-10 surfactant, the displacement efficiency improved from 68.32% to 72.02%, reflecting an increase of 3.7%. The minimum pore size associated with this segment of NP-10 surfactant displacement was determined to be 0.02 μm. The statistical data regarding oil displacement efficiency are presented in Table 5. The diagram illustrating oil displacement efficiency can be found in Figure 13. The T2 spectrum is depicted in Figure 14. The pore diameter characteristics associated with varying displacement PV numbers are illustrated in Figure 15. Additionally, the on-line NMR imaging features corresponding to different displacement PV numbers are shown in Figure 16.

Table 5. Statistical analysis of oil displacement efficiency.

Serial Number	Semaphore Signaling Mechanism	Displacement Efficacy (%)	Export Assessment
Saturated oil	13,112.76797		\
Water displacement: 1 PV	10,743.60803	18.07	Oil: 0.5 mL; Water: 2.4 mL
Water displacement: 3 PV	7372.014108	43.78	Oil: 1.3 mL; Water: 7.5 mL
Water displacement: 15 PV	4154.704748	68.32	Oil: 2.0 mL; Water: 43.1 mL
NP-10 displacement: 1 PV	3940.328825	69.95	Oil: 2.1 mL; Water: 46.0 mL
NP-10 displacement: 3 PV	3796.351371	71.05	Oil: 2.2 mL; Water: 51.5 mL
NP-10 displacement: 5 PV	3703.289228	71.76	Oil: 2.2 mL; Water: 57.8 mL
NP-10 displacement: 10 PV	3668.95556	72.02	Oil: 2.2 mL; Water: 73.3 mL

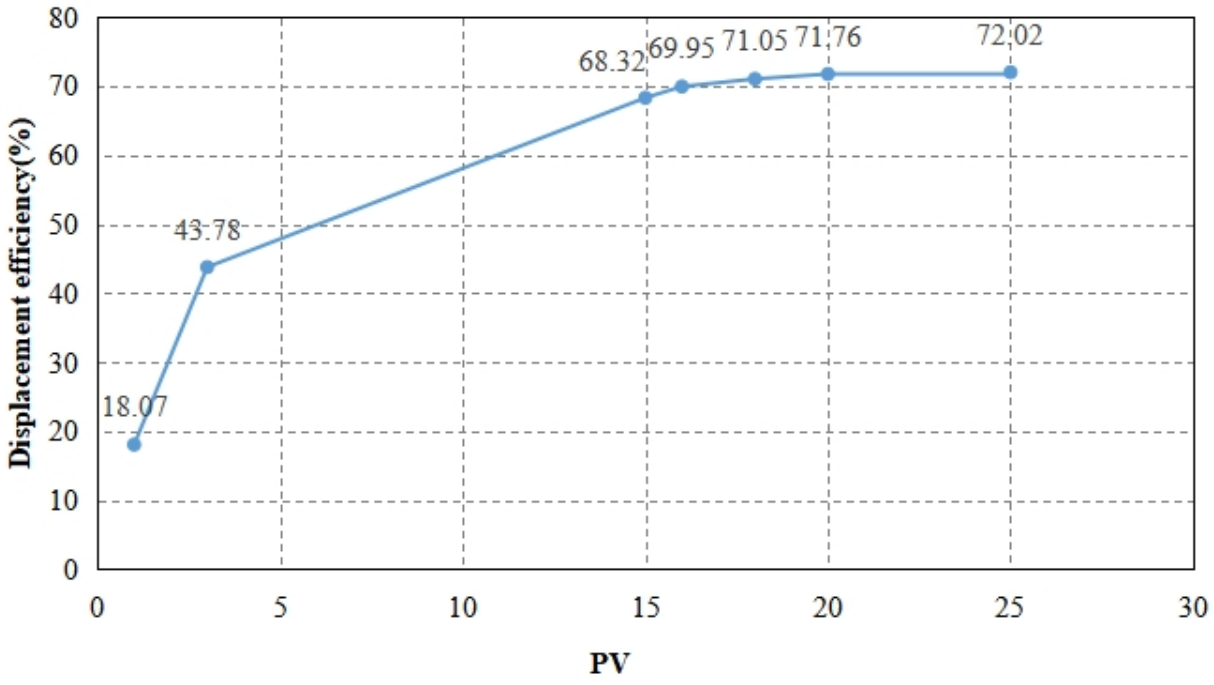

Figure 13. Displacement efficiency diagram for the "water displacement + NP-10 surfactant displacement".

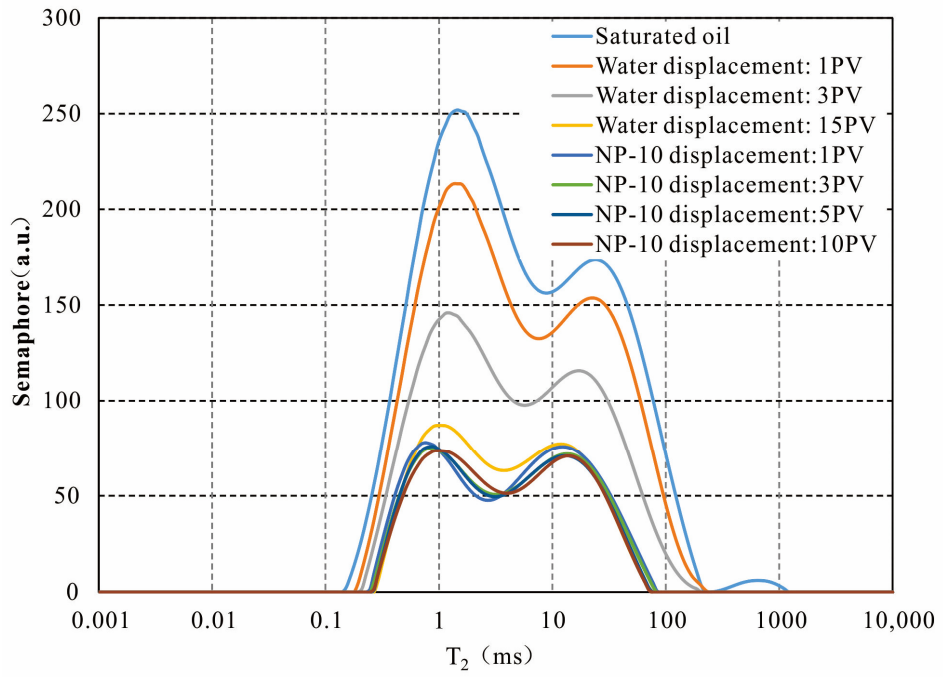

Figure 14. NMR T2 spectral characteristics corresponding to different PV numbers of "water displacement + NP-10 surfactant displacement".

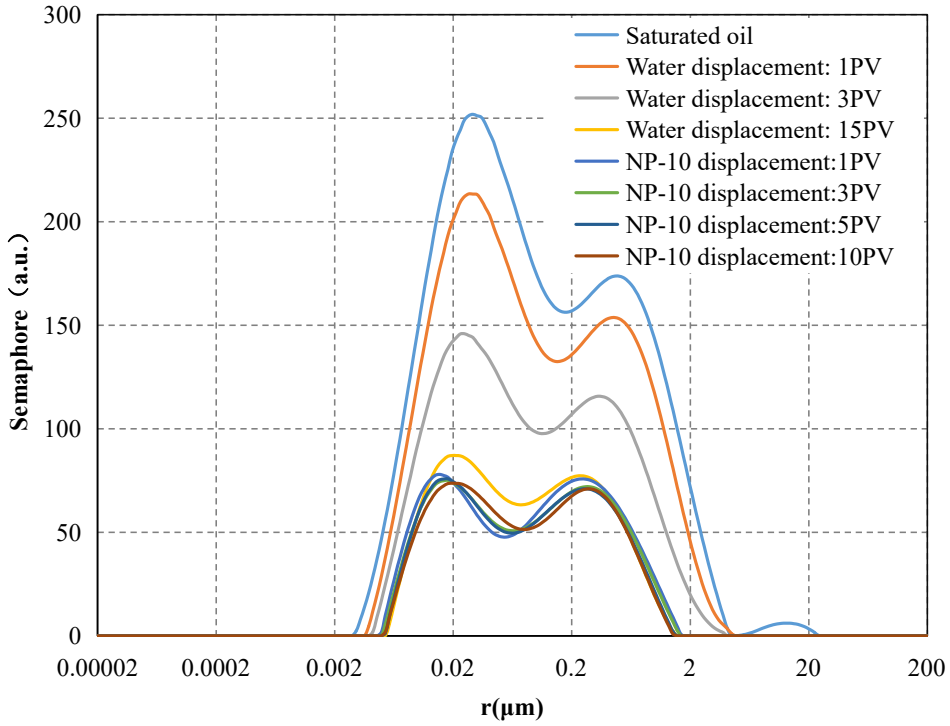

Figure 15. Oil displacement pore size characteristics corresponding to different PV numbers of "water displacement + NP-10 surfactant displacement".

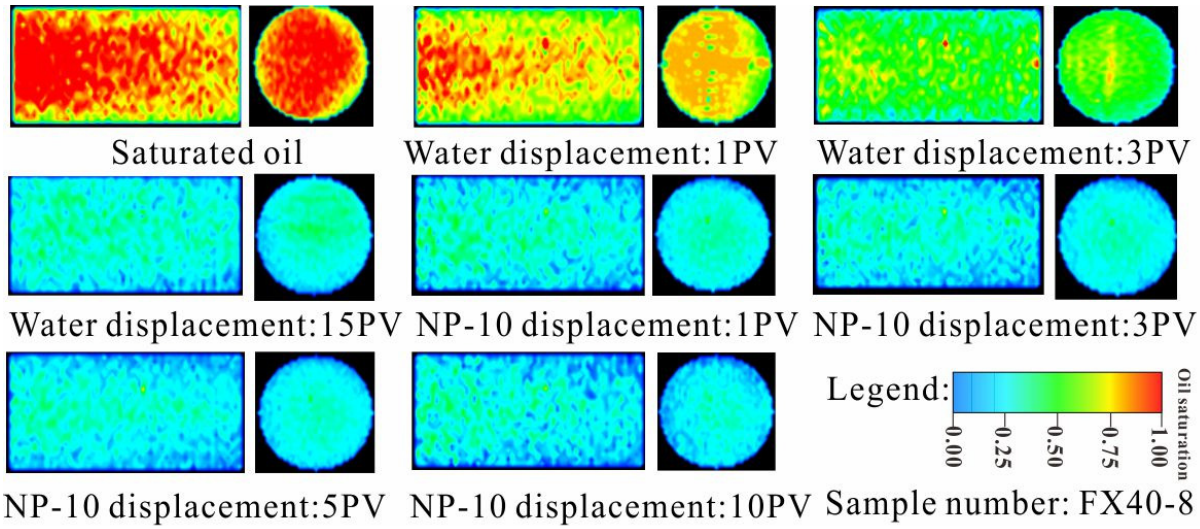

Figure 16. On-line NMR imaging characteristics corresponding to different PV numbers of "water displacement + NP-10 surfactant displacement".

For the FX40-9 sample, water displacement was initially performed, followed by oil displacement using a 0.4% mass concentration of the FSD-952 surfactant. The oil displacement efficiency remained unchanged at a water displacement PV number of 15 PV, indicating that the maximum water displacement efficiency had been achieved. At this juncture, the displacement of the superficial activator FSD-952, with a mass concentration of 0.4%, commenced. The results indicate that during the process of water displacement, oil displacement predominantly occurs in medium-to-large pores. When the water displacement reaches 5 pore volumes (PV), there is a slight enhancement in the water displacement effect; at 15 PV, this effect peaks at 69.93%. Subsequently, a water displacement experiment utilizing a surfactant concentration of 0.4% mass FSD-952 was conducted. This led to the mobilization of oil within pores as small as 0.03 μm, resulting in an increase in displacement efficiency from 69.93% to 74.77% when the surfactant's application reached 10 PV. The minimum pore diameter associated with crude oil displaced using FSD-952 surfactant at a concentration of 0.4% was noted to be approximately 0.03 μm. The statistical data regarding oil displacement efficiency are presented in Table 6. The diagram illustrating oil displacement efficiency can be found in Figure 17. The T2 spectrum is depicted in Figure 18. The pore size characteristics associated with various displacement PV numbers are illustrated in Figure 19. Additionally, the on-line NMR imaging features corresponding to different displacement PV numbers are shown in Figure 20.

Table 6. Statistical analysis of oil displacement efficiency.

Serial Number	Semaphore Signaling Mechanism	Displacement Efficacy (%)	Export Assessment
Saturated oil	12,520.55878		\
Water displacement: 1 PV	9979.569271	20.29	Oil: 0.6 mL; Water: 2.2 mL
Water displacement: 3 PV	6607.750386	47.22	Oil: 1.3 mL; Water: 7.2 mL
Water displacement: 15 PV	3764.514041	69.93	Oil: 1.9 mL; Water: 42.1 mL
FSD-952 displacement: 1 PV	3480.752139	72.20	Oil: 2.0 mL; Water: 44.2 mL
FSD-952 displacement: 3 PV	3316.6376	73.51	Oil: 2.1 mL; Water: 50.0 mL
FSD-952 displacement: 5 PV	3208.011019	74.38	Oil: 2.1 mL; Water: 55.8 mL
FSD-952 displacement: 10 PV	3158.338058	74.77	Oil: 2.2 mL; Water: 70.8 mL

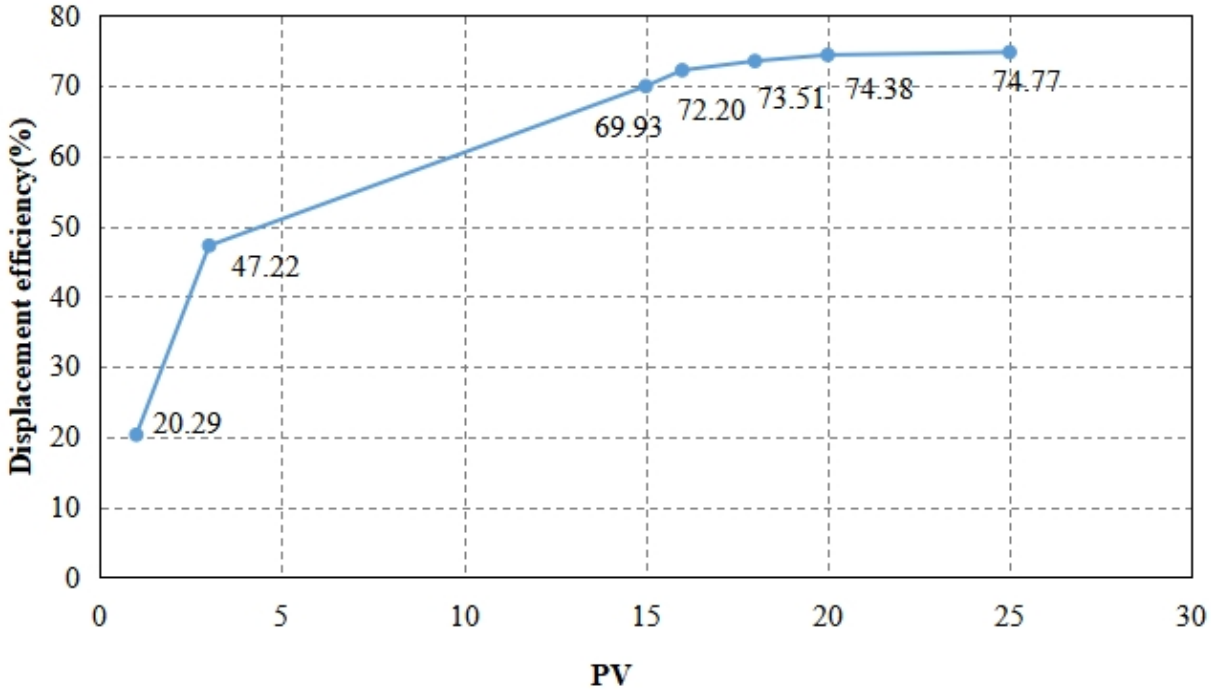

Figure 17. Displacement efficiency diagram for the "water displacement + FSD-952 surfactant displacement".

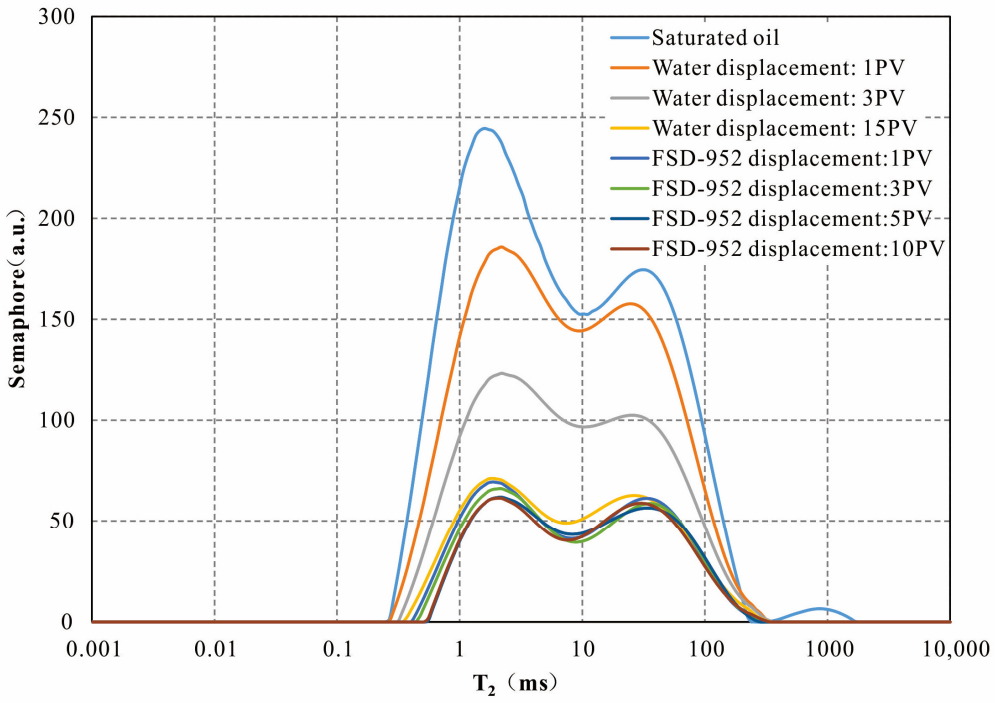

Figure 18. NMR T_2 spectral characteristics corresponding to different PV numbers of "water displacement + FSD-952 surfactant displacement".

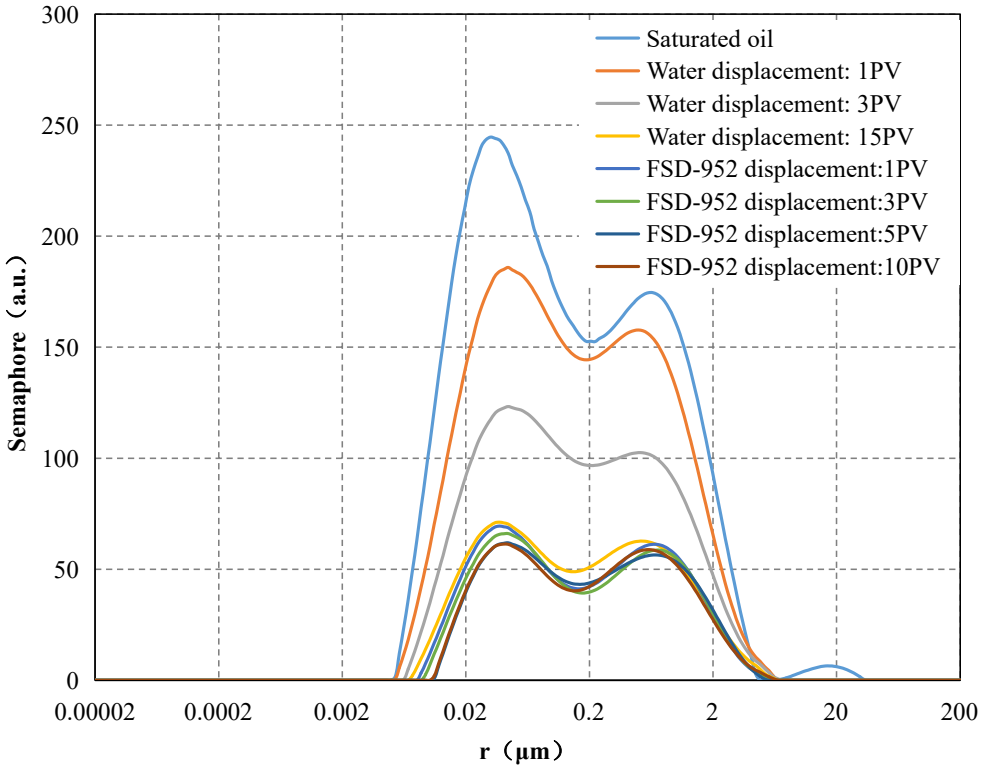

Figure 19. Oil displacement pore size characteristics corresponding to different PV numbers of "water displacement + FSD-952 surfactant displacement".

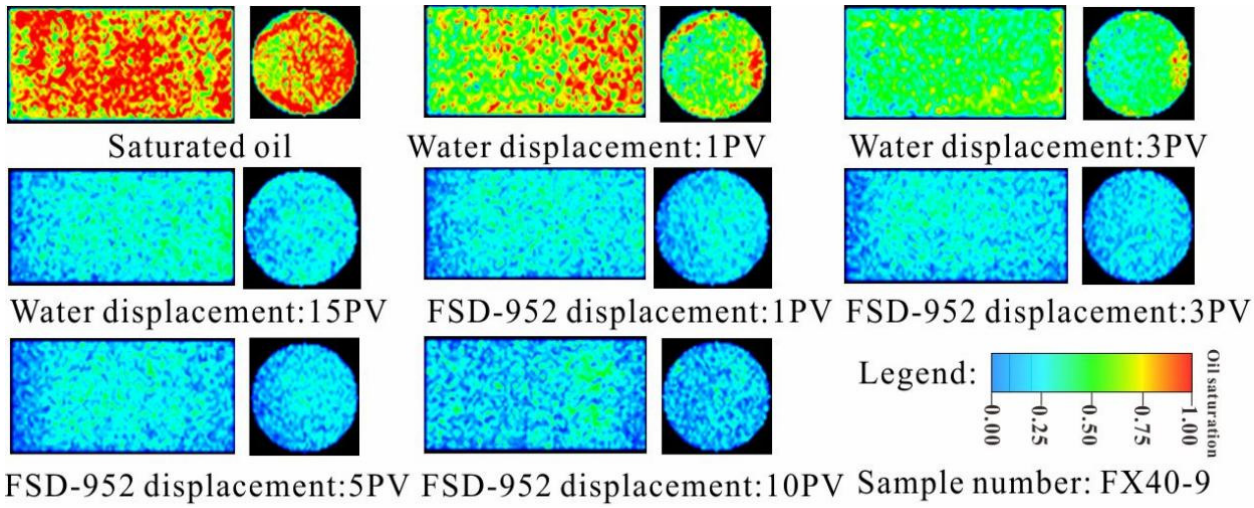

Figure 20. On-line NMR imaging characteristics corresponding to different PV numbers of "water displacement +FSD-952 surfactant displacement".

4. Conclusions

(1) This finding indicates the presence of an optimal surfactant concentration, with NP-10 achieving its minimum interfacial tension at a concentration of 0.1%. Similarly, GPHQ-1 also exhibits a minimum interfacial tension at this same concentration, whereas FSD-952 reaches its minimum at a higher concentration of 0.4%. Notably, GPHQ-1 demonstrates the lowest recorded interfacial tension value of 0.0762 mN/m.

(2) In terms of oil displacement efficiency and enhancement, the ranking is GPHQ-1 > FSD-952 > NP-10. The oil displacement efficiencies for the surfactants GPHQ-1, FSD-952, and NP-10 exhibited increases of 6.67%, 4.81%, and 3.7%, respectively. The

minimum pore sizes corresponding to the displacements facilitated by GPHQ-1, NP-10, and FSD-952 were determined to be 0.01 μm, 0.02 μm, and 0.03 μm, respectively.

(3) In the context of developing the Fuxian Chang 8 reservoir, the GPHQ-1 surfactant is utilized to perform displacement tests, specifically aimed at extracting crude oil confined within small pore spaces.

Author Contributions: Formal analysis, H.Y.; Data curation, J.L. and Y.W.; Writing – original draft, G.Z. All authors have read and agreed to the published version of the manuscript.

Funding: This research was funded by the Natural Science Basic Research Program of Shaanxi Province, China (2024JC-YBQN-0341).

Data Availability Statement: The original contributions presented in the study are included in the article, further inquiries can be directed to the corresponding author.

Acknowledgments: We acknowledge the State Key Laboratory of Continental Dynamics for assisting with the completion of this project.

Conflicts of Interest: Author H.Y. was employed by the company Fuxian Oil Production Plant, Yanchang Oilfield Co., Ltd. The remaining authors declare that the research was conducted in the absence of any commercial or financial relationships that could be construed as a potential conflict of interest.

References

1. Zhao, X.; Liao, G.; Liu, W.; Peng, B.; Luan, H.; Chen, Q.; Su, X.; Feng, Y. New advances in surfactant EOR mechanism: Micellar solubilization and in-situ emulsification. *Sci. Sin. Chim.* **2023**, *53*, 1088–1103.
2. Hou, Z. Influence of Surfactant Molecular Structure on Oil/Water Interface Aggregation Behavior and Oil Displacement Efficiency. Ph.D. Thesis, Northeast Petroleum University, Daqing, China, 2023.
3. Gao, X.; Zhang, L.; Li, J.; Zhou, X.; Zhao, X.; Lyu, T. Chemical Analysis of Surfactants and Experimental Study on Improving Oilfield Recovery. *Contemp. Chem. Ind.* **2023**, *52*, 2931–2934.
4. Hou, X.; Lu, Y.; Fang, B.; Zhang, F.; Hu, G. Research progress on application of surfactants in unconventional oil and gas stimulation. *Petrochem. Technol.* **2023**, *52*, 734–741.
5. Kang, W.; Wang, K.; Li, Z.; Lv, W.; Yang, H.; Jia, R.; He, Y. Study on slow-release surfactant nanocarriers in low-permeability reservoirs. *China Surfactant Deterg. Cosmet.* **2022**, *52*, 1147–1154.
6. Liu, H.; Cai, X.; Tian, F.; Zheng, Y.; Lu, X.; Lan, L. Synthesis of fluorocarbon surfactant and development of its compound surfactant system for depressurization and increasing injection. *Chem. Eng. Oilgas* **2022**, *51*, 84–90.
7. Li, W.; Li, Z.; Zhang, D.; Zhang, C.; Li, Y. Highly Stable Supercritical CO_2 Foam with Zwitterionic Surfactant and Nanoparticle as Foaming Agents for Channeling Blocking. *Oilfield Chem.* **2024**, *41*, 101–107.
8. Han, X.; Wei, L.; Liu, W.; Bai, Y. Impact of Oil-Displacing Agent on the Emulsification Stability of Oily Wastewater in Alkali-Free Ternary Composite Flooding. *Appl. Chem. Ind.* **2024**, *53*, 1817.
9. Li, Z.; Pu, D.; Xiong, Y.; Wu, D.; Jin, C.; Guo, Y. Research progress of nanomaterials for oil displacement in enhancing oil recovery. *Chem. Ind. Eng. Prog.* **2023**, *43*, 5035.
10. Bera, A.; Belhaj, H. Application of nanotechnology by means of nanoparticles and nanodispersions in oil recovery—A comprehensive review. *J. Nat. Gas Sci. Eng.* **2016**, *34*, 1284–1309. [CrossRef]
11. Liu, H.; Jin, X.; Ding, B. Application of nanotechnology in petroleum exploration and development. *Pet. Explor. Dev.* **2016**, *43*, 1107–1115. [CrossRef]
12. Eltoum, H.; Yang, Y.; Hou, J. The effect of nanoparticles on reservoir wettability alteration: A critical review. *Pet. Sci.* **2021**, *18*, 136–153. [CrossRef]
13. Wang, C. Applied Basic Research and Adaptability Evaluation of Surfactant Flooding in Ultra-Low Permeability Reservoirs. Ph.D. Thesis, Shaanxi University of Science and Technology, Xi'an, China, 2018.
14. Yang, J.; Huang, Z.; Dong, X.; Liu, Y. Surfactant Oil Displacement System Research of Ansai Oilfield. *Oilfield Chem.* **2015**, *32*, 559–563.
15. Chen, G.; Song, Y.-P.; Tang, D.-Y.; Zhao, J.-R. Evaluation and Application of a New Surfactant Oil-Displacing Agent in Low Permeability Oilfield. *Oilfield Chem.* **2014**, *31*, 410–418.
16. Li, G.; Yang, W.; Wei, J.; Zhao, G.; Qing, X.; Wang, Y. Analysis on Chemical Mechanism of Surfactant Flooding and Experimental Study on Reducing Pressure and Increasing Injection. *Contemp. Chem. Ind.* **2023**, *52*, 2947–2949.
17. Roldán-Carrillo, T.; Gladys-Castorena, C.; Salazar-Castillo, R.O.; Hernández-Escobedo, L.; Olguín-Lora, P.; Gachuz-Muro, H. Hybrid low salinity water and surfactant process for enhancing heavy oil recovery. *Pet. Explor. Dev.* **2023**, *50*, 1278–1288. [CrossRef]

18. Wei, B.; Wang, Y.; Zhao, J.; Kadet, V.; Pu, W. Influence laws of solid-liquid interface characteristics on the imbibition behaviors of tight/shale reservoirs: A case study of tight reservoirs in Member 7 and 8 of Yanchang Formation and shale reservoirs in Longmaxi Formation. *Acta Pet. Sin.* **2023**, *44*, 1683–1692.
19. Peng, Y.; Qv, C.; Xv, C. Enhanced Oil Recovery Technology of Modified Surfactant Flooding in Low-permeability Reservoirs in Yanchang Oilfield. *Contemp. Chem. Ind.* **2022**, *51*, 1302–1310.
20. Hu, J.; Jin, C.; Shi, L.; Guo, Y. Surface active-polymer flooding agent for medium and low permeability reservoir. *Fine Chem.* **2023**, *40*, 2064–2072.
21. Du, M.; Yang, Z.; Lyu, W.; Li, Z.; Wang, G.; Chen, X.; Qi, X.; Yao, L.; Zhang, Y.; Jia, N.; et al. Experiment of dynamic seepage in tight/shale reservoirs under matrix fracture coupling. *Pet. Explor. Dev.* **2024**, *51*, 403–415. [CrossRef]
22. Bai, S.; Cheng, D.; Wan, J.; Yang, L.; Peng, H.; Guo, X.; Zeng, J. Quantitative characterization of sandstone NMR T2 spectrum. *Acta Pet. Sin.* **2016**, *37*, 382.
23. Zhong, G.; Wu, Y.; Wang, S.; Li, Y.; Lei, K.; Li, Y.; Yang, S. Review on the application of nuclear magnetic resonance technology in carbon dioxide geological sequestration and utilization. *Prog. Geophys.* **2024**, *39*, 0225–0240. (In Chinese)
24. Li, Q.; Li, Q.; Wang, F.; Wu, J.; Wang, Y. The Carrying Behavior of Water-Based Fracturing Fluid in Shale Reservoir Fractures and Molecular Dynamics of Sand-Carrying Mechanism. *Processes* **2024**, *12*, 2051. [CrossRef]
25. Li, Q.; Li, Q.; Han, Y. A Numerical Investigation on Kick Control with the Displacement Kill Method during a Well Test in a Deep-Water Gas Reservoir: A Case Study. *Processes* **2024**, *12*, 2090. [CrossRef]

Disclaimer/Publisher's Note: The statements, opinions and data contained in all publications are solely those of the individual author(s) and contributor(s) and not of MDPI and/or the editor(s). MDPI and/or the editor(s) disclaim responsibility for any injury to people or property resulting from any ideas, methods, instructions or products referred to in the content.